Solubility and Diffusivity of Hydrofluorocarbons in Room-Temperature Ionic Liquids

Mark B. Shiflett
DuPont Central Research and Development, Experimental Station E304, Wilmington, DE 19880

A. Yokozeki
DuPont Fluoroproducts Laboratory, Chestnut Run, Plaza 711, Wilmington, DE 19880

DOI 10.1002/aic.10685
Published online October 13, 2005 in Wiley InterScience (www.interscience.wiley.com).

*Gaseous absorption measurements of hydrofluorocarbons (trifluoromethane, difluoromethane, pentafluoroethane, 1,1,1,2-tetrafluoroethane, 1,1,1-trifluoroethane, and 1,1-difluoroethane) in l-*n*-butyl-3-methylimidazolium hexafluorophosphate ([bmim][PF_6]) and 1-*n*-butyl-3-methylimidazolium tetrafluoroborate ([bmim][BF_4]) were performed using a gravimetric microbalance at various isothermal conditions (temperatures between 283.15 and 348.15 K) and at pressures < 2 MPa. This report shows for the first time the solubility and diffusivity data for the hydrofluorocarbons in room-temperature ionic liquids and surprisingly large differences in the solubility among the hydrofluorocarbons. Experimental gas solubility data were successfully correlated with well-known solution models (Margules, Wilson, and NRTL activity coefficient equations). Diffusivities obtained from the time-dependent absorption data were well analyzed using a diffusivity model developed in this study. The present solubility and diffusivity data are also compared with those of CO_2, studied in our previous study.*
AIChE J, 52: 1205–1219, 2006
Keywords: ionic liquid, hydrofluorocarbons, solubility, diffusivity, phase equilibria

Introduction

Room-temperature ionic liquids (or, simply called *ionic liquids*) are molten salts composed of organic cations and inorganic anions. Although they have been known since 1914,[1] the research activities on this new type of liquids increased dramatically with the development of the first air-stable and nearly moisture-stable tetrafluoroborate $[BF_4]^-$ ionic liquids in 1992.[2] Now, various ionic liquids have even been commercially available since 1999.[3]

Because of the extremely large possible combinations of ions—approximately 10^{18} pairs[4]—ionic liquids are truly designer solvents. This large number of possible combinations can be used to optimize production costs and thermophysical properties such as solubility, melting points, thermal stability, electric conductivity, and thermal conductivity, to cite several. Another unique feature of ionic liquids is practically a lack of vapor pressure, and thus emissions in engineering applications will be significantly lower than those for conventional volatile organic solvents. Therefore, ionic liquids are often called "green solvents" (or environmentally friendly solvents), although sufficient toxicological information is missing at present.

Because this class is a new type of solvent, there are numerous possible applications that will replace conventional solvents or provide something novel with respect to applications. Whatever the applications will be, a fundamental knowledge about the thermophysical properties of their mixtures with various chemicals is critically important and needed: for example, solubility of various compounds in ionic liquids with

Correspondence concerning this article should be addressed to A. Yokozeki at akimichi.yokozeki@usa.dupont.com.

Table 1. Constants for α in Eq. 5

Binary System	α (dimensionless)
CO_2/[bmim][PF_6]	0.750
CO_2/[bmim][BF_4]	0.750
R-32/[bmim][PF_6]	0.756
R-32/[bmim][BF_4]	0.750
R-23/[bmim][PF_6]	0.875
R-125/[bmim][PF_6]	0.531
R-134a/[bmim][PF_6]	0.594
R-143a/[bmim][PF_6]	0.588
R-152a/[bmim][PF_6]	0.650

various thermodynamic conditions (T, P, x: temperature, pressure, composition) and transport/electric properties such as viscosity, diffusivity, thermal conductivity, and electric conductivity. These property measurements as well as theoretical understandings of such properties are largely lacking at present.

In this study, we investigate the solubility and diffusivity of various hydrofluorocarbons (HFCs) in two room-temperature ionic liquids: [bmim][PF_6] and [bmim][BF_4]. HFCs studied here are trifluoromethane (R-23), difluoromethane (R-32), pentafluoroethane (R-125), 1,1,1,2-tetrafluoroethane (R-134a), 1,1,1-trifluoroethane (R-143a), and 1,1-difluoroethane (R-152a). HFCs belong to an important class of compounds in various industrial and household applications. They have been developed as alternative compounds as a result of the environmental concern of chlorofluorocarbons and hydrochlorofluorocarbons, which were used for refrigerants, blowing agents, propellants, solvents, cleaning agents, fire extinguisher agents, medical applications, and so forth. The present study is the first systematic investigation of the HFC solubility and diffusivity in ionic liquids; only a couple of works on HFCs in ionic liquids have so far been reported in the literature such as very high pressure solubilities of R-23[5] and electrochemical applications of R-32 or R-134a (no solubility data).[6,7]

The observed solubility data will be analyzed with the conventional solution (activity coefficient) models for nonelectrolyte solutions such as Margules, Wilson, and nonrandom two-liquid (NRTL) models,[8,9] and it will be shown that the nonelectrolyte models work very well in the phase-equilibrium correlation, even for the ionic-liquid electrolyte solutions. The observed behaviors (diffusivity vs. P, or diffusivity vs. composition x) of the diffusivity data in ionic liquids are successfully explained by a simple semitheoretical model developed in this study. The solubility and diffusivity of CO_2/ionic-liquid solutions in our previous study[10] are also compared with the present HFC results.

Experimental Procedures and Results

Materials and experiment

The [bmim][PF_6] (Lot and Filling code, 1055432 31304010) and [bmim][BF_4] (Lot and Filling Code, 1080045 11304079) were obtained from Fluka Chemika (Buchs, Switzerland) with a purity of >96 and >97%, respectively. The chloride content was measured by ion chromatography, and the extractable chloride content as purchased for [bmim][PF_6] and [bmim][BF_4] was 4.7 and 1.6 g m^{-3}, respectively. R-23, R-32, R-125, R-134a, R-143a, and R-152a were obtained from DuPont Fluoroproducts (Wilmington, DE) with a minimum purity of 99.9%. A molecular sieve trap was installed to remove trace amounts of water from the gases. Special care was taken to use separate molecular sieve traps for each gas to prevent cross-contamination.

The gas solubility and diffusivity measurements were made using a gravimetric microbalance (Hiden Isochema Ltd, IGA 003) as described in our previous report.[10] Initially, 60 to 80 mg of ionic liquid was loaded into the sample container and heated to 348.2 K under a vacuum of about 10^{-9} MPa for 10 h to remove any trace amounts of water or other impurities. Four isotherms were measured at 283.2 (or 285.2), 298.2, 323.2, and 348.2 K over a pressure range from about 0.01 to 2.0 MPa. The upper pressure limit for each gas was dependent on the saturation pressure in the sample container at ambient temperature. To ensure sufficient time for gas–liquid equilibrium, the ionic liquid samples were maintained at each pressure set point for a minimum of 3 h with a maximum time-out of 10 h. Additional experimental details are provided in Shiflett and Yokozeki.[10]

Error analysis

The instrumental uncertainties in T and P are within 0.1 K and 0.8 kPa, respectively. These errors do not cause any significant changes in the gas solubility (mole fraction) measurement. One of the largest sources of error in the present experiment is data reproducibility. We have examined the data reproducibility by repeating the experiments over different times (for example, one month apart for the same binary system). Our best estimate for the present experimental reproducibility error, including the sample (ionic liquid) purity effect, has been <0.005 mole fraction. The next largest systematic error is attributed to the buoyancy correction in the data analysis.

When gas dissolves in ionic liquid, the liquid volume will change. The change in liquid volume affects the buoyancy force in the gravimetric microbalance. Here we estimate a systematic error (or the correction term) in solubility (mole fraction) as a result of neglecting the volume change of a gas-dissolved ionic liquid. A volume (V_L) of gas-dissolved liquid may safely be assumed to be a mole fraction average of molar volumes of each constituent species, given that we are interested in only a minor correction term:

$$V_L = \tilde{V}_1 \frac{w_1}{M_1} + \tilde{V}_0 \frac{w_0}{M_0} \tag{1}$$

where subscripts 1 and 0 represent a sample gas and an ionic liquid, respectively; w is the amount of weight in the liquid mixture; M is molar mass; and $\tilde{V}$ is the molar saturated-liquid volume at a given temperature T.

A liquid volume change δV_L, arising from the gas absorption amount δw_1, is

$$\delta V_L = \frac{\tilde{V}_1}{M_1} \delta w_1 \tag{2}$$

Then, the actual weight reading (w_1) in the microbalance must be corrected by adding the buoyancy effect (a small amount of weight, δw_1) attributed to δV_L:

Table 2. Experimental Solubility (T, P, x) and Diffusivity (D) Data of R-32*

(1) R-32/(2) [bmim][PF_6]				(1) R-32/(2) [bmim][BF_4]			
T (K)	P (MPa)	$100x_1$ (mol %)	D ($\times 10^{-11}$) (m^2 s^{-1})	T (K)	P (MPa)	$100x_1$ (mol %)	D ($\times 10^{-11}$) (m^2 s^{-1})
283.2	0.0098	2.6	—	283.1	0.0100	0.9	1.8
283.2	0.0996	10.6	1.9	283.1	0.0998	9.9	1.7
283.2	0.2497	27.1	1.7	283.2	0.2499	24.1	3.3
283.2	0.3996	42.8	3.6	283.2	0.3995	37.4	4.5
283.2	0.5497	55.8	6.3	283.0	0.5499	50.1	8.5
283.2	0.6996	68.0	7.4	283.1	0.6999	62.7	11
283.2	0.8495	81.5	6.1	283.1	0.8497	75.9	10
298.1	0.0097	1.8	—	298.2	0.0097	0.7	3.4
298.2	0.0995	7.6	2.4	298.2	0.0997	7.1	3.4
298.2	0.2497	19.0	2.4	298.2	0.2496	17.5	3.7
298.2	0.3998	29.7	3.5	298.2	0.3999	27.2	4.6
298.1	0.5497	39.0	5.4	298.2	0.5498	35.9	6.0
298.1	0.6995	47.5	6.7	298.2	0.6996	43.8	7.4
298.2	0.8501	55.2	8.3	298.2	0.8495	51.5	9.1
298.1	0.9999	62.8	8.8	298.2	0.9999	58.8	9.9
322.8	0.0099	0.6	4.8	323.2	0.0098	0.4	8.7
323.1	0.0995	4.7	5.3	323.1	0.0996	4.0	7.6
323.1	0.2496	11.3	5.3	323.2	0.2497	9.9	7.4
323.1	0.3995	17.4	6.0	323.2	0.3996	15.4	8.2
323.1	0.5497	23.1	6.0	323.1	0.5496	20.6	9.0
323.1	0.6996	28.5	7.7	323.1	0.6995	25.5	9.9
323.2	0.8496	33.5	8.5	323.0	0.8499	30.1	11
323.2	0.9996	38.2	—	323.2	0.9996	34.5	11
348.2	0.0099	0.3	7.1	348.2	0.0097	0.2	13
348.2	0.0997	2.9	8.2	348.1	0.0996	2.4	13
348.2	0.2495	7.0	8.1	348.1	0.2495	5.8	13
348.2	0.3994	10.9	9.8	348.2	0.3995	9.2	12
348.1	0.5498	14.6	9.7	348.1	0.5495	12.5	15
348.1	0.6997	18.2	9.6	348.2	0.6996	15.6	16
348.2	0.8496	21.4	9.6	348.1	0.8496	18.6	14
348.2	0.9999	24.8	12	348.1	0.9999	21.4	19

*—, Erratic time-dependent data: not analyzed for D.

$$\delta w_1 = \frac{\tilde{V}_1}{M_1}\,\delta w_1 \rho_g(T, P) = \tilde{V}_1 \delta w_1 \tilde{\rho}_g \tag{3}$$

where $\rho_g(T, P)$ is a superheated gas density at the system T and P, and $\tilde{\rho}_g$ is the corresponding molar density, which can be calculated as well as $\tilde{V}_1$ by a REFPROP computer code.[11] After some algebraic manipulations, Eq. 3 can be converted to a molar correction term, δx_1:

$$\delta x_1 = x_1(1 - x_1)\tilde{\rho}_g \tilde{V}_1 \tag{4}$$

For example, using actual experimental data of $x_1 = 0.8121$ (uncorrected mole fraction) for a R-32 (1)/[bmim][PF_6] (2) system at 283.2 K and 0.8495 MPa, Eq. 4 gives the correction term of 0.0033 mole fraction, where $\tilde{\rho}_g = 0.0004194$ mol cm^{-3} and $\tilde{V}_1 = 51.021$ cm^{-3} mol from REFPROP.[11]

Thus, the systematic error arising from the volume change in the liquid solution can be corrected with Eq. 4, as long as $\tilde{\rho}_g$ and $\tilde{V}_1$ are known. Unfortunately, $\tilde{V}_1$ is calculated only for temperatures $< T_c$ (critical temperature of gaseous species 1) with REFPROP[11] (or any equations of state). Because some of our experimental conditions exceed T_c, a proper method to estimate $\tilde{V}_1$ in all temperatures including those above T_c has to be developed. Here, we propose the following simple equation of $\tilde{V}_1$ for all temperatures:

$$\tilde{V}_1 = (1 - \alpha)\tilde{V}_0 \tag{5}$$

where $\tilde{V}_0$ is a molar liquid volume of ionic liquid at T and α is a unique temperature-independent constant for each binary system, described below.

For [bmim][PF_6], $\tilde{V}_0$ is given by

$$\tilde{V}_0\,[\mathrm{cm^3/mol}] = \frac{M_0}{\rho_L} = \frac{284.18}{1.619874 - 8.441224 \times 10^{-4} T\,[\mathrm{K}]} \tag{6}$$

and for [bmim][BF_4]

$$\tilde{V}_0\,[\mathrm{cm^3/mol}] = \frac{M_0}{\rho_L} = \frac{226.02}{1.412932 - 7.056735 \times 10^{-4} T\,[\mathrm{K}]} \tag{7}$$

Coefficients in ρ_L (liquid density of ionic liquid) were obtained by fitting experimental liquid densities of ionic liquids.[10] Equation 5 is based on our previous report,[10] where we have found a molar liquid volume of a mixture, $\tilde{V}_m$, can be well correlated with the following simple equation:

Table 3. Experimental Solubility (T, P, x) and Diffusivity (D) Data of R-125 and R-134a*

(1) R-125/(2) [bmim][PF_6]				(1) R-134a/(2) [bmim][PF_6]			
T (K)	P (MPa)	$100x_1$ (mol %)	D ($\times 10^{-11}$) (m^2 s^{-1})	T (K)	P (MPa)	$100x_1$ (mol %)	D ($\times 10^{-11}$) (m^2 s^{-1})
283.1	0.0099	1.3	—	283.0	0.0100	0.3	0.4
283.2	0.0996	3.4	—	283.2	0.0498	5.0	0.6
283.3	0.1996	7.5	0.6	283.1	0.0999	12.6	0.6
283.2	0.2996	12.6	0.9	283.1	0.1498	21.3	1.0
283.3	0.3996	18.5	1.6	283.1	0.2002	30.5	1.5
283.1	0.4997	25.5	2.4	283.1	0.2491	40.4	2.7
283.2	0.5997	34.2	4.0	283.1	0.2997	51.9	5.3
283.1	0.6996	46.2	6.1	283.1	0.3490	72.4	3.6
283.2	0.7998	66.0	8.6				
298.2	0.0098	0.3	—	298.2	0.0100	1.1	—
298.2	0.0996	2.3	1.8	298.1	0.0498	4.2	1.9
298.2	0.1998	5.0	1.5	298.2	0.0997	8.6	1.7
298.1	0.2995	8.0	2.1	298.2	0.1499	13.0	2.0
298.2	0.3998	11.1	2.0	298.2	0.1993	17.6	2.3
298.2	0.4995	14.3	2.4	298.1	0.2500	22.4	2.6
298.2	0.5995	18.0	2.6	298.2	0.2995	27.5	2.8
298.2	0.7996	26.1	4.8	298.1	0.3500	32.6	4.0
298.1	0.9998	36.3	7.8				
323.1	0.0100	0.0	—	323.1	0.0099	0.4	2.4
323.1	0.0996	1.3	4.3	323.2	0.0498	2.1	4.4
323.1	0.1998	2.8	4.6	323.1	0.0997	4.3	3.9
323.2	0.3000	4.2	5.2	323.1	0.1499	6.5	4.5
323.1	0.3997	5.7	4.7	323.2	0.1990	8.7	4.4
323.2	0.4999	7.2	5.4	323.2	0.2490	10.9	—
323.1	0.5996	8.7	5.1	323.2	0.2990	13.1	4.9
323.1	0.7997	12.0	5.5	323.2	0.3493	15.4	5.0
323.1	0.9996	15.4	5.9				
348.2	0.0102	0.0	—	348.2	0.0097	0.0	6.4
348.1	0.0997	0.7	7.5	348.1	0.0498	0.9	7.5
348.2	0.1996	1.6	9.5	348.1	0.0993	2.2	7.9
348.3	0.2997	2.5	7.0	348.1	0.1501	3.5	7.8
348.2	0.3997	3.3	8.0	348.2	0.1998	4.7	8.4
348.2	0.4998	4.3	9.9	348.2	0.2501	5.9	8.4
348.2	0.5998	5.3	7.1	348.2	0.3002	7.2	8.3
348.3	0.8000	7.0	11	348.2	0.3490	8.5	—
348.2	0.9996	8.8	8.9				

*—, Erratic time-dependent data: not analyzed for D.

$$\frac{\Delta \tilde{V}}{\tilde{V}_0} \equiv \frac{\tilde{V}_m}{\tilde{V}_0} - 1 \approx -\alpha x_1 \tag{8}$$

where α (>0) is nearly independent of temperatures (even for those $>T_c$). Then, if we assume $\tilde{V}_m$ is equal to a mole fraction average of each constituent molar volume, Eq. 5 can be derived. Estimated values in α from the slope in the plot of Eq. 8 are shown in Table 1.

Although Eq. 5 is a rough estimate, it is sufficient for the present purpose because we are dealing here with a minor correction term using Eq. 4. We have estimated a systematic error attributed to the use of the approximation Eq. 5 to be <0.002 mole fraction, comparing the results with the use of the accurate $\tilde{V}_1$ ($<T_c$ of REFPROP[11]]. Thus, total errors in the solubility data arising from both random and systematic errors have been estimated to be <0.006 mole fractions at given T and P.

Concerning errors in the diffusivity data, the largest error source comes from experimental reproducibility (random) errors. They were estimated to be roughly within a factor of two in the determined diffusivity, based on the scatters of various analyzed diffusivity data. The second largest error source in the diffusivity data is ascribed to the assumed liquid-depth parameter L (see the following section for the diffusivity result) in the analysis, which was assumed to be constant. However, L varies with the amount of gas absorption, resulting from the liquid expansion by the gas absorption. Errors by this variable L in the analysis showed $\lesssim$60% effect in the final diffusivity data. Thus, the overall error limit in the diffusivity of a factor of two, cited above, will cover this systematic error as well.

Results

The present solubility [VLE (T, P, x)] data are summarized in Tables 2–5, and Table 5 contains the previous result[10] of CO_2/[bmim][PF_6] for comparison. Figure 1 shows a plot of normalized pressures (or more precisely, normalized-fugacities at 298.2 K) vs. molar compositions, which measures the deviation from the ideal solubility behavior (Raoult's law). Surprisingly large differences in the solubility among the same family of compounds (HFCs) are clearly observed, such as from a slightly negative deviation in R-32 to a highly positive deviation in R-143a. These behaviors are quite unexpected.

Although Henry's law constants do not tell the whole story about actual solubility behaviors of gases, they are often reported in the literature as the limiting solubility at infinite dilution. The Henry's law constant (H) is defined as

Table 4. Experimental Solubility (T, P, x) and Diffusivity (D) Data of R-143a and R-152a*

(1) R-143a/(2) [bmim][PF_6]				(1) R-152a/(2) [bmim][PF_6]			
T (K)	P (MPa)	$100x_1$ (mol %)	D ($\times 10^{-11}$) (m^2 s^{-1})	T (K)	P (MPa)	$100x_1$ (mol %)	D ($\times 10^{-11}$) (m^2 s^{-1})
284.9	0.0096	0.3	—	283.2	0.0097	2.1	—
285.2	0.0997	2.9	—	283.2	0.0499	10.3	1.1
285.1	0.1983	6.1	0.8	283.2	0.0993	21.0	1.6
285.2	0.2974	9.4	—	283.2	0.1499	30.2	3.1
285.5	0.3981	12.5	1.0	283.1	0.2001	40.9	3.6
285.2	0.4998	15.9	1.1	283.1	0.2495	52.3	6.4
285.2	0.5982	19.2	1.4	283.1	0.3196	79.9	—
285.4	0.6998	22.4	1.9				
285.4	0.7483	24.1	2.0				
298.2	0.0095	0.4	—	298.2	0.0100	3.0	—
298.1	0.0997	2.3	—	298.2	0.0501	7.7	2.0
298.1	0.2005	4.2	—	298.1	0.0998	13.6	2.6
298.1	0.2990	6.9	1.8	298.2	0.1492	19.5	2.9
298.1	0.4015	9.1	1.8	298.2	0.2497	31.2	5.0
298.1	0.4989	11.4	2.2	298.2	0.3482	43.5	7.7
298.1	0.5986	13.6	2.7	298.2	0.4505	57.7	10
298.1	0.7002	15.9	2.8				
298.1	0.7501	16.9	3.6				
323.1	0.0105	0.1	—	323.3	0.0099	0.7	5.7
323.1	0.1002	1.3	4.5	323.3	0.0501	3.0	—
323.3	0.2005	2.7	3.4	323.2	0.1002	6.0	5.5
323.2	0.3000	4.1	2.9	323.2	0.1502	8.9	5.9
323.2	0.4002	5.4	5.1	323.2	0.2497	14.6	6.4
323.2	0.5005	6.8	4.1	323.3	0.3495	20.1	—
323.2	0.6004	8.1	3.8	323.2	0.4505	25.6	7.9
323.2	0.7003	9.4	5.6				
323.2	1.0003	13.1	5.5				
348.2	0.0099	0.0	—	348.1	0.0103	0.5	14
348.1	0.1000	0.9	7.4	348.1	0.0502	1.8	13
348.0	0.1996	1.8	10	348.1	0.1002	3.5	12
348.1	0.3000	2.7	11	348.1	0.1501	5.3	13
348.1	0.4002	3.6	13	348.2	0.2496	8.6	14
348.1	0.5003	4.5	12	348.2	0.3497	11.8	15
348.2	0.5998	5.4	14	348.0	0.4500	15.0	—
348.2	0.7003	6.3	—				
348.1	1.0004	8.6	—				

*—, Erratic time-dependent data: not analyzed for D.

$$H = \lim_{x \to 0} \frac{f(T, P, y)}{x} \tag{9}$$

where f is the vapor-phase fugacity of solute (vapor composition, y) at the system T and P, x is the liquid-phase solute mole fraction, and y is the vapor-phase solute mole fraction.

In the present case, $f(T, P, y)$ can be treated as the pure vapor fugacity of the solute species ($y = 1$), resulting from the negligible vapor pressure of ionic liquids. However, Eq. 9 introduces a problem because it becomes indeterminate (that is, approaches 0/0) at the limit ($x = 0$). This problem can be resolved by the use of l'Hôpital's rule, which gives

$$H \approx \left(\frac{df}{dx} \right)_{x=0} \tag{10}$$

where f is an empirically fitted fugacity as a function of x at each isotherm; here we have used a second-order polynomial function for f. Henry's law constants thus obtained are shown in Table 6, where previous results for CO_2/ionic liquids are also listed for comparison.

Diffusivity (D) was obtained from the analysis of time-dependent absorption data, $\langle C \rangle$, using the following model equation[10,12]:

$$\langle C \rangle = C_s \left[1 - 2 \left(1 - \frac{C_0}{C_s} \right) \sum_{n=0}^{\infty} \frac{\exp(-\lambda_n^2 D t)}{L^2 \lambda_n^2} \right] \tag{11}$$

where $\lambda_n = [n + (1/2)](\pi/L)$; C_0 and C_s are the initial and final concentrations of a solution mixture, respectively; and L is the liquid depth of the solution in a test container. Detailed procedures of the analysis are given in Shiflett and Yokozeki.[10] The results are shown in Tables 2–5, together with the solubility (T, P, x) data.

Data Correlation

In this section, we first analyze the experimental solubility (T, P, x) data with the existing solution models for nonelectrolyte solutions, which may also be applied even for electrolyte solutions, particularly for the case of the phase-boundary correlation (such as vapor–liquid equilibria).[13-16] In fact, all observed solubility behaviors in the present ionic solutions have been well correlated using the well-known solubility models for nonelectrolyte

Table 5. Experimental Solubility (T, P, x) and Diffusivity (D) Data of R-23 and CO_2*

(1) R-23/(2) [bmim][PF_6]				(1) CO_2/(2) [bmim][PF_6]			
T (K)	P (MPa)	$100x_1$ (mol %)	D ($\times 10^{-11}$) (m^2 s^{-1})	T (K)	P (MPa)	$100x_1$ (mol %)	D ($\times 10^{-11}$) (m^2 s^{-1})
282.6	0.0500	1.0	1.5	283.1	0.0097	0.4	—
282.8	0.1098	2.8	—	283.1	0.0501	1.6	2.0
282.6	0.4000	11.3	1.5	283.1	0.1002	2.9	2.2
282.6	0.7000	20.0	2.2	283.6	0.3996	10.2	2.6
282.6	0.9993	28.4	2.9	283.8	0.6996	16.7	3.0
282.7	1.2997	36.5	4.3	283.7	1.0000	22.4	3.6
282.6	1.4996	41.9	5.7	282.1	1.3003	28.4	—
283.1	2.0002	53.5	—	283.1	1.4998	30.9	—
				283.1	1.9998	37.9	5.2
298.1	0.0497	0.8	2.6	298.1	0.0102	0.0	—
298.1	0.0999	1.8	3.2	298.1	0.0502	0.9	5.1
298.1	0.3993	7.9	2.4	298.1	0.1002	1.8	4.8
298.1	0.6995	13.8	3.0	298.2	0.3996	7.2	4.5
298.0	1.0004	19.5	4.0	298.2	0.7000	12.2	5.4
298.1	1.3006	25.0	3.9	298.1	0.9994	16.7	5.7
298.1	1.5000	28.4	5.7	298.1	1.2999	20.8	6.8
298.1	1.9999	37.3	7.1	298.1	1.4994	23.3	7.7
				298.1	1.9992	29.1	8.1
323.1	0.0098	0.0	6.3	323.3	0.0102	0.2	11
323.1	0.0498	0.5	6.3	323.2	0.0503	0.6	11
323.1	0.0996	1.1	7.3	323.2	0.1002	1.2	9.7
323.1	0.3996	5.0	5.9	323.3	0.3996	4.7	10
323.2	0.7004	8.6	6.7	323.2	0.7000	7.9	10
323.1	1.0004	12.1	8.0	323.2	0.9998	10.9	13
323.2	1.2993	15.6	7.5	323.2	1.3002	13.6	13
323.1	1.5001	17.9	12	323.3	1.5003	15.5	14
323.2	1.9993	23.1	11	323.2	1.9998	19.7	15
348.1	0.0096	0.1	—	348.2	0.0102	0.1	—
348.1	0.0497	0.3	8.1	348.1	0.0501	0.2	24
348.1	0.0997	0.8	12	348.1	0.1000	0.7	21
348.1	0.3997	3.3	10	348.1	0.3997	3.2	28
348.1	0.7002	5.7	—	348.1	0.7000	5.6	24
348.1	0.9993	8.0	11	348.0	1.0002	7.8	—
348.0	1.3003	10.5	—	348.2	1.3003	9.9	—
348.1	1.4994	12.0	—	348.1	1.4999	11.3	—
348.1	2.0000	14.9	23	348.3	1.9995	14.9	28

*—, Erratic time-dependent data: not analyzed for D.

solutions. Next, in the diffusivity model subsection, we develop a semitheoretical model for diffusivity data of general solutions and apply it successfully to the present diffusivity data.

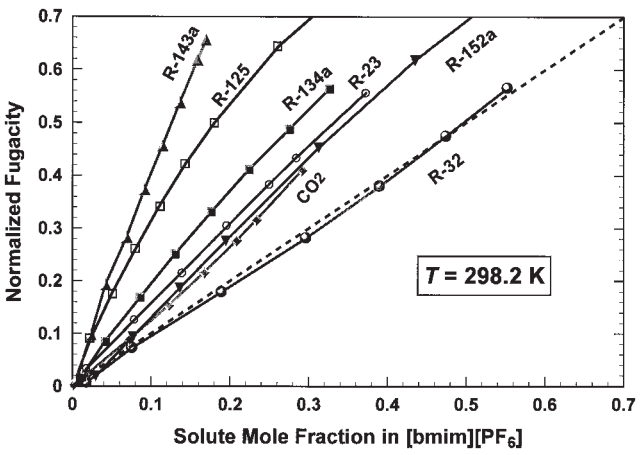

Figure 1. Normalized fugacities vs. compositions at 298.2 K.

The fugacity is normalized by that in the saturated liquid of the pure solute. The dashed line represents Raoult's law.

Solubility model

In general, low- and medium-pressure VLE (vapor liquid equilibria) for an N-component system can be described by[17]

$$y_i P \Phi_i = x_i \gamma_i P_i^s \qquad (i = 1, \ldots, N) \tag{12}$$

where y is the vapor-phase mole fraction, x is the liquid-phase mole fraction, P is system pressure, P_i^s is the saturated vapor pressure of the ith species, γ is the activity coefficient (function of compositions and T), and Φ_i is a correction factor for the ith species ($\approx$1 for sufficiently low P systems).

For a binary system ($N = 2$) of gas (1)/ionic liquid (2) mixtures, it is reasonable to assume that $y_1 = 1$ (or $y_2 = 0$) at temperatures of the present interest (that is, $P_2^s \approx 0$). Then, the activity coefficient for species 1 is given by Eq. 12:

$$\gamma_1 = \frac{P \Phi_1}{x_1 P_1^s} \tag{13}$$

For the present case[17] the correction factor Φ_1 is

Table 6. Henry's Law Constants in bar (10 × MPa)

Binary System	T = 283.2 K	T = 298.2 K	T = 323.2 K	T = 348.2 K
CO_2/[bmim][PF_6]*	34.9 ± 0.2	51.7 ± 0.3	81.6 ± 0.4	121.1 ± 0.4
CO_2/[bmim][BF_4]*	36.6 ± 0.2	55.0 ± 0.3	86.2 ± 0.3	130.9 ± 0.4
R-23/[bmim][PF_6]	32.9 ± 0.4	48.8 ± 0.4	77.6 ± 0.7	110.6 ± 3.7
R-32/[bmim][PF_6]	8.8 ± 0.7	11.9 ± 0.4	20.6 ± 0.1	34.1 ± 0.1
R-32/[bmim][BF_4]	9.4 ± 0.4	13.4 ± 0.2	24.0 ± 0.1	41.5 ± 0.4
R-125/[bmim][PF_6]	23.1 ± 2.3	38.8 ± 2.7	73.8 ± 1.5	112.1 ± 4.5
R-134a/[bmim][PF_6]	7.8 ± 2.4	11.8 ± 0.1	23.4 ± 0.2	45.7 ± 0.1
R-143a/[bmim][PF_6]	32.6 ± 0.7**	44.1 ± 3.5	72.1 ± 0.7	106.9 ± 4.3
R-152a/[bmim][PF_6]	5.5 ± 1.6	7.7 ± 2.1	16.5 ± 0.1	27.9 ± 0.3

* Taken from Shiflett and Yokozeki.[10]
**At T = 285.2 K.

$$\Phi_1 = \exp\left[\frac{(B_1 - \tilde{V}_1)(P - P_1^s)}{RT}\right] \tag{14}$$

where B_1 is the second virial coefficient of species 1 at system T, $\tilde{V}_1$ is the saturated molar liquid volume of species 1 at system T, and R is the universal gas constant.

$B_1(T)$ can be obtained, for example, from Yokozeki et al.[18] or by a REFPROP computer code[11] and similarly $\tilde{V}_1$ can be calculated if T is less than the critical point T_c of a pure component 1. In the present analysis, however, we adopt an approximate $\tilde{V}_1$, which was defined earlier by Eq. 5, and can be applied even for temperatures $> T_c$. It should be mentioned here that the present approximate $\tilde{V}_1$ in Eq. 5 is sufficient for the present data analysis with Eqs. 12–14 because it is used merely in the correction term Φ_1.

With respect to the vapor pressure of pure species 1, we use an Antoine-type equation for temperature variations:

$$\ln P_1^s = A_1 - \frac{B_1}{T + C_1} \tag{15}$$

Coefficients in Eq. 15 were determined by fitting P_1^s (from REFPROP[11]) between 283.2 and 348.2 K (or T_c), shown in Table 7, and we assume that Eq. 15 holds even above T_c as an extrapolated hypothetical vapor pressure.

Now, we are ready to analyze experimental solubility data using the activity coefficient of Eq. 13. For each isothermal solubility datum, the activity coefficients γ_1 were calculated at each observed x_1 point. Several activity models are available in the literature.[8,9] In this work, we examined three commonly used models: the two-parameter Margules, Wilson, and NRTL equations. The activity coefficients by the Margules model are

$$\ln \gamma_1 = [A + 2(B - A)x_1]x_2^2 \tag{16}$$

$$\ln \gamma_2 = [B + 2(A - B)x_2]x_1^2 \tag{17}$$

A, B adjustable binary interaction parameters (18)

In the case of the Wilson model

$$\ln \gamma_1 = -\ln(x_1 + \Lambda_{12}x_2) + x_2\left(\frac{\Lambda_{12}}{x_1 + \Lambda_{12}x_2} - \frac{\Lambda_{21}}{\Lambda_{21}x_1 + x_2}\right) \tag{19}$$

$$\ln \gamma_2 = -\ln(x_2 + \Lambda_{21}x_1) - x_1\left(\frac{\Lambda_{12}}{x_1 + \Lambda_{12}x_2} - \frac{\Lambda_{21}}{\Lambda_{21}x_1 + x_2}\right) \tag{20}$$

where

Table 7. Constants in Eq. 15*

Species 1	A_1	B_1	C_1
CO_2	12.3312	4759.46	156.462
R-32	9.49117	3006.86	37.1416
R-23	14.8971	7416.05	257.365
R-125	9.15935	2966.36	37.4124
R-134a	8.10384	2432.86	−12.331
R-143a	9.07017	3001.73	41.4509
R-152a	7.97275	2433.85	−11.4809

*Pressure unit in MPa and temperature unit in K.

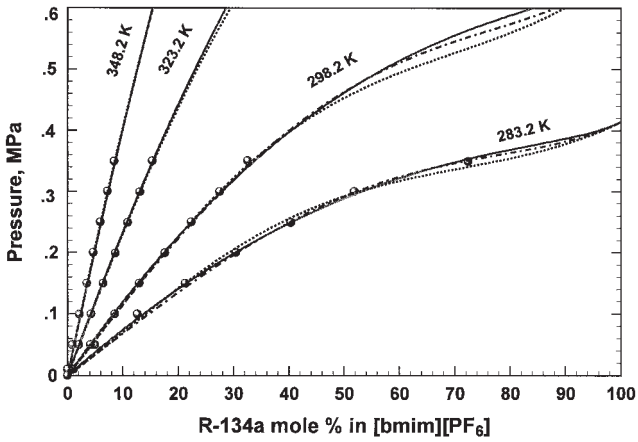

Figure 2. Isothermal *P–x* (solubility) diagram for R-134a/[bmim][PF_6] mixtures.

Solid lines: Wilson activity model; dotted lines: NRTL model; broken lines: Margules model. Symbols: the present experimental data.

Table 8. Determined Parameters of Eq. 30 for the NRTL Activity-Coefficient Model

System (1)/(2)	$\tau_{12}^{(0)}$	$\tau_{12}^{(1)}$ (K)	$\tau_{21}^{(0)}$	$\tau_{21}^{(1)}$ (K)	δP (MPa)*
CO_2/[bmim][PF_6]	−4.663	2806.8	1.0656	−812.37	0.0078
CO_2/[bmim][BF_4]	−2.454	2209.6	0.8119	−723.52	0.0076
R-23/[bmim][PF_6]	4.303	−313.31	−0.1424	−353.02	0.0168
R-32/[bmim][PF_6]	4.408	−565.89	−1.0275	−199.06	0.0067
R-32/[bmim][BF_4]	0.6154	714.11	0.5525	−674.40	0.0078
R-125/[bmim][PF_6]	2.788	−78.28	1.2041	−422.79	0.0084
R-134a/[bmim][PF_6]	−3.001	1699.2	2.5102	−1000.0	0.0043
R-143a/[bmim][PF_6]	6.266	−251.81	−0.1725	−53.31	0.0043
R-152a/[bmim][PF_6]	−2.506	1834.4	1.9383	−1000.0	0.0058

*Standard deviations in pressure of the nonlinear regression analysis with $\alpha = 0.2$ (see text).

$$\Lambda_{12} \equiv \frac{V_2^L}{V_1^L}\exp(-\lambda_{12}) \qquad \text{and} \qquad \Lambda_{21} \equiv \frac{V_1^L}{V_2^L}\exp(-\lambda_{21}) \tag{21}$$

$$\lambda_{12} \equiv \frac{\Delta\lambda_1}{RT} \qquad \text{and} \qquad \lambda_{21} \equiv \frac{\Delta\lambda_2}{RT}$$

(adjustable binary interaction parameters) (22)

and V_i^L is the molar volume of pure liquid component i.

In the case of the NRTL model

$$\ln \gamma_1 = x_2^2\left[\tau_{21}\left(\frac{G_{21}}{x_1 + x_2 G_{21}}\right)^2 + \frac{\tau_{12}G_{12}}{(x_2 + x_1 G_{12})^2}\right] \tag{23}$$

$$\ln \gamma_2 = x_1^2\left[\tau_{12}\left(\frac{G_{12}}{x_2 + x_1 G_{12}}\right)^2 + \frac{\tau_{21}G_{21}}{(x_1 + x_2 G_{21})^2}\right] \tag{24}$$

where

$$G_{12} \equiv \exp(-\alpha\tau_{12}) \qquad \text{and} \qquad G_{21} \equiv \exp(-\alpha\tau_{21}) \tag{25}$$

$$\tau_{12} \equiv \frac{\Delta g_1}{RT} \qquad \text{and} \qquad \tau_{21} \equiv \frac{\Delta g_2}{RT}$$

(adjustable binary interaction parameters) (26)

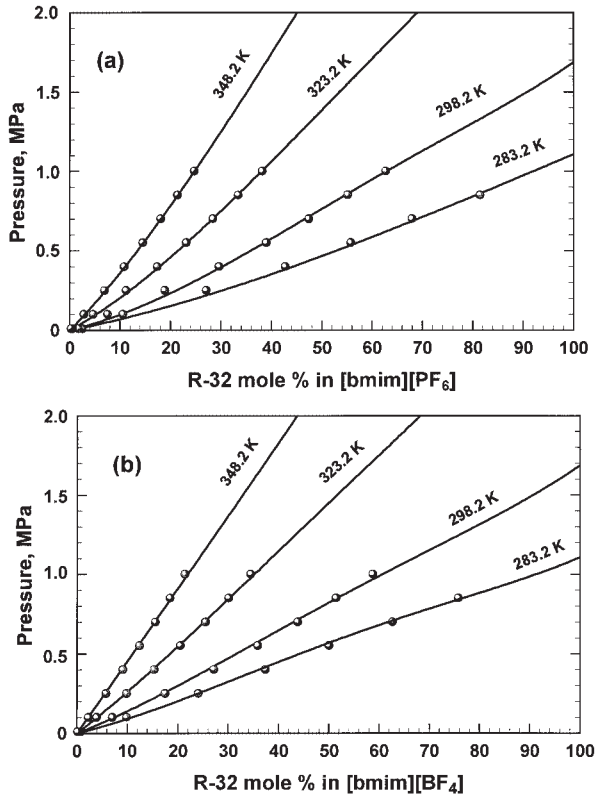

Figure 3. Isothermal *P–x* (solubility) diagrams.

Lines: NRTL model calculations; symbols: the present experimental data. (a) R-32/[bmim][PF_6]; (b) R-32/[bmim][BF_4].

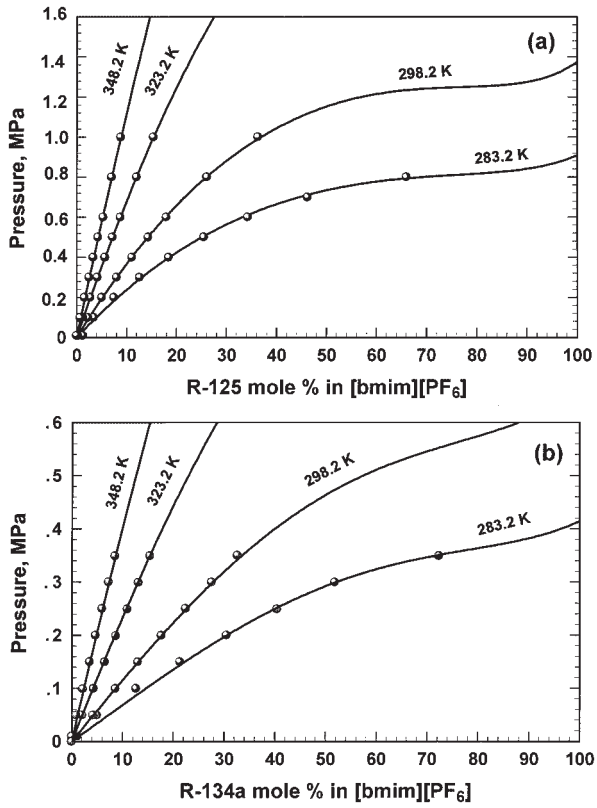

Figure 4. Isothermal *P–x* (solubility) diagrams.

Lines: NRTL model calculations; symbols: the present experimental data. (a) R-125/[bmim][PF_6]; (b) R-134a/[bmim][PF_6].

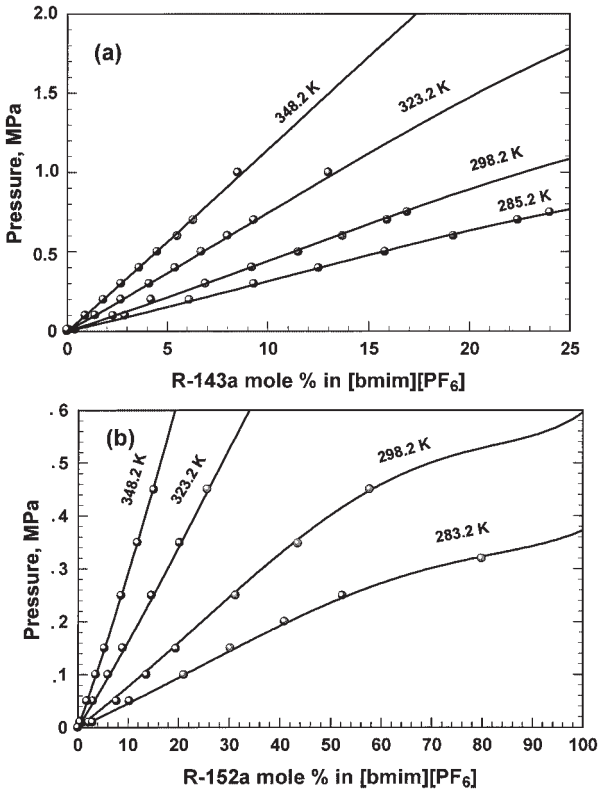

Figure 5. Isothermal *P–x* (solubility) diagrams.

Lines: NRTL model calculations; symbols: the present experimental data. (a) R-143a/[bmim][PF_6]; (b) R-152a/[bmim][PF_6].

and $\alpha = 0.2$ (assumed to be a constant of 0.2 in this work).

The temperature-dependent binary interaction parameter (p_{ij}) is often modeled by[8,16]

$$p_{ij} = p_{ij}^{(0)} + p_{ij}^{(1)}/T + p_{ij}^{(2)}T \tag{27}$$

In this study, we have modeled all p_{ij} by the first two terms for Eqs. 18, 22, and 26:

$$A = A^{(0)} + A^{(1)}/T \quad \text{and} \quad B = B^{(0)} + B^{(1)}/T \tag{28}$$

$$\lambda_{12} = \lambda_{12}^{(0)} + \lambda_{12}^{(1)}/T \quad \text{and} \quad \lambda_{21} = \lambda_{21}^{(0)} + \lambda_{21}^{(1)}/T \tag{29}$$

$$\tau_{12} = \tau_{12}^{(0)} + \tau_{12}^{(1)}/T \quad \text{and} \quad \tau_{21} = \tau_{21}^{(0)} + \tau_{21}^{(1)}/T \tag{30}$$

The adjustable parameters in Eqs. 28–30 can be obtained by fitting Eq. 13 with the activity coefficient models of Eq. 16 (Margules), Eq. 19 (Wilson), or Eq. 23 (NRTL).

Another method to obtain the binary interaction parameters is to fit the experimental pressure data directly. The calculation of pressures at a given T can be made using Eqs. 13 and 14 with the proper activity coefficient model (Eq. 16, 19, or 23), although P is not a pressure-explicit form. This requires iterative calculations; a Newton–Raphson method works very well here. From Eqs. 13 and 14, the implicit pressure equation is

$$\ln P + (P - P_1^s)(B_1 - \tilde{V}_1)/RT - \ln P_1^s - \ln(x_1\gamma_1) = 0 \tag{31}$$

where P_1^s is given by Eq. 15; $\tilde{V}_1$ is given by Eq. 5; γ_1 is calculated by Eq. 16, 19, or 23; and B_1 can be obtained from Yokozeki et al.[18] or a REPPROP program.[11]

We have analyzed the experimental solubility data using both methods (Eqs. 13 and 31) and found that both analyses give equivalent results. Therefore, in this report, we show only the results with the pressure-fitting method (using Eq. 31). In addition, the three activity-coefficient models (Margules, Wilson, and NRTL) provided equally good data correlation. Figure 2 shows an example for the comparison of isothermal *P–x* plots using the R-134a/[bmim][PF_6] system. The binary interaction parameters used in Figure 2 are $A^{(0)} = 2.512$, $A^{(1)} = -541.47$ K, $B^{(0)} = 0.2439$, and $B^{(1)} = 357.10$ K in Eq. 28; $\lambda_{12}^{(0)} = 1.6894$, $\lambda_{12}^{(1)} = -261.25$ K, $\lambda_{21}^{(0)} = 0.8232$, and $\lambda_{21}^{(1)} = 138.46$ K in Eq. 29; and $\tau_{12}^{(0)} = -3.001$, $\tau_{12}^{(1)} = 1699.2$ K, $\tau_{21}^{(0)} = 2.5102$ and $\tau_{21}^{(1)} = -1000.0$ K in Eq. 30, respectively. Standard deviations in the pressure fit are 0.004, 0.005, and 0.004 MPa for the Margules, Wilson, and NRTL models, respectively. With respect to the VLE correlation, the three models were equally acceptable for all binary systems studied here. However, the Margules equation is a good model but purely empirical (that is, simply empirical polynomials), whereas both Wilson and NRTL activity coefficients have some theoretical foundations, although the Wilson model is applicable only for VLE [that is, no liquid–liquid equilibrium (LLE) prediction].[8] In this article, we

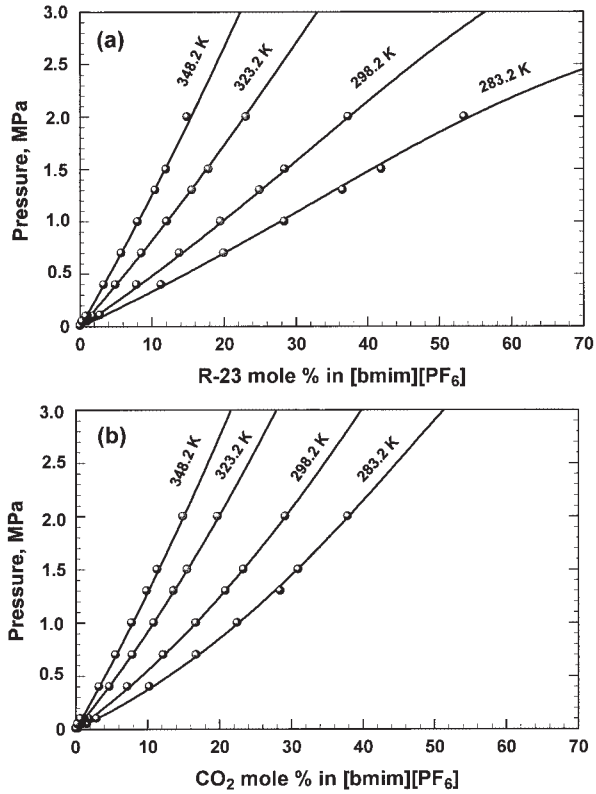

Figure 6. Isothermal *P–x* (solubility) diagrams.

Lines: NRTL model calculations; symbols: the present experimental data. (a) R-23/[bmim][PF_6]; (b) CO_2/[bmim][PF_6].

Table 9. Coefficients in Eq. 37*

Compound i	A_i	B_i (K)	C_i (K^{-1})	D_i (K^{-2})	Reference
CO_2	−3.097	48.86	2.381×10^{-2}	-7.480×10^{-5}	9
R-23	−12.2443	1000.535	4.68401×10^{-2}	-8.5150×10^{-5}	11
R-32	4.738618	−461.5	-1.80359×10^{-2}	0	24
R-125	−1.66528	550.0	-7.13348×10^{-3}	0	24
R-134a	−6.0481	906.845	1.09872×10^{-2}	-2.1031×10^{-5}	25
R-143a	−16.0625	1480.0	5.81055×10^{-2}	-9.4414×10^{-5}	11
R-152a	−5.98879	876.463	7.63641×10^{-3}	-1.1078×10^{-5}	11
[bmim][PF_6]	50.2168	0	-2.47304×10^{-1}	3.14162×10^{-4}	10
[bmim][BF_4]	−10.50897	4238.641	0	0	10

*Viscosity in mPa · s (or cP), and T in K.

report the results of the solubility correlation only with the NRTL model.

Determined binary interaction parameters in Eq. 30 are listed in Table 8 for the present binary systems as well as our previous CO_2/ionic liquids.[10] Isothermal P–x diagrams calculated with these parameters are compared with observed values in Figures 3–6.

Diffusivity model

A diffusion coefficient D_{AB}, of a dilute solute A (spherical body with a radius r_A) in a solvent B (viscosity η_B), is given by the Einstein–Stokes equation[9,19]:

$$D_{AB} = \frac{kT}{6\pi r_A \eta_B} \tag{32}$$

where k is the Boltzmann constant and T is temperature.

This equation may be a starting point in developing empirical correlations for diffusivity data in general liquid solutions. In addition, it is well known empirically that the mutual diffusion coefficient D in liquid is correlated with the solution viscosity η; $D \propto \eta^{-n}$, where usually $0.5 \leq n \leq 1$ for various compounds.[9] Then, we propose the following empirical form as a modified Einstein–Stokes equation:

$$D = \frac{kT}{6\pi r \eta_0 (\eta/\eta_0)^b} \tag{33}$$

or

$$\ln(D/T) = a - b \ln(\eta/\eta_0) \tag{34}$$

where $a = \ln(k/6\pi r\eta_0)$ and η_0 is a unit viscosity (such as 1 Pa·s in SI units); this unit viscosity is needed as a normalization factor for the equation to have the proper dimension. When $b = 1$ and $a = \ln(k/6\pi r_A)$, Eq. 33 becomes Eq. 32. Thus, the proposed equation can be regarded as a generalized Einstein–Stokes equation for a general solution with adjustable parameters a and b. With respect to the solution viscosity in Eq. 34, we adopt our earlier model for an N-component solution viscosity[20]:

$$\ln(\eta/\eta_0) = \sum_{i=1}^{N} \xi_i \ln(\eta_i/\eta_0) \tag{35}$$

where

$$\xi_i = m_i^c x_i \Big/ \sum_{i=1}^{N} m_i^c x_i \tag{36}$$

and where m_i is the molecular weight of the ith species, x_i is the mole fraction of the ith species, η_i is the dynamic viscosity of the ith species, c is an adjustable parameter, and η_0 is the unit viscosity to render the equation dimensionless. It is instructive to note that if $c = 1$, Eq. 36 represents a mass fraction, whereas if $c = 0$, then it is simply a mole fraction. The usefulness of Eq. 35 has been discussed in Michels and Sienel.[21] The present diffusivity model, Eq. 34 with Eq. 35, has three empirical adjustable parameters (a, b, and c) to correlate observed diffusivity data (function of x, and T), provided that the viscosity of each pure species is known. The dynamic viscosity of a pure compound i is modeled as

$$\ln \eta_i = A_i + \frac{B_i}{T} + C_i T + D_i T^2 \tag{37}$$

Coefficients in Eq. 37 for several compounds studied here are given in Table 9.

The adjustable parameter c is nonlinear in Eqs. 34 and 35, and we have found it is a rather insensitive parameter to the correlation with values between 0 and 1. Thus, instead of using a nonlinear regression analysis, we used several fixed trial values in c between 0 and 1, and then applied a linear regression analysis of Eq. 34 to obtain the parameters a and b. Determined parameters for several systems are listed in Table 10 and model calculations with these parameters are compared with experimental diffusivity data in Figures 7–11, where the pressure axis was calculated by the P–x diagram of the NRTL

Table 10. Determined Parameters in Eqs. 34 and 36

System	a	b	c
CO_2/[bmim][PF_6]	−26.466 ± 0.153	0.691 ± 0.041	0.7
CO_2/[bmim][BF_4]	−26.724 ± 0.094	0.641 ± 0.031	0.7
R-23/[bmim][PF_6]	−27.334 ± 0.120	0.658 ± 0.037	0.3
R-32/[bmim][PF_6]	−28.245 ± 0.127	0.422 ± 0.047	0.5
R-32/[bmim][BF_4]	−27.794 ± 0.076	0.565 ± 0.032	0.5
R-125/[bmim][PF_6]	−27.602 ± 0.116	0.697 ± 0.038	0.2
R-134a/[bmim][PF_6]	−27.472 ± 0.157	0.752 ± 0.045	0.7
R-143a/[bmim][PF_6]	−27.066 ± 0.150	0.893 ± 0.047	0.0
R-152a/[bmim][PF_6]	−27.244 ± 0.104	0.697 ± 0.034	0.5

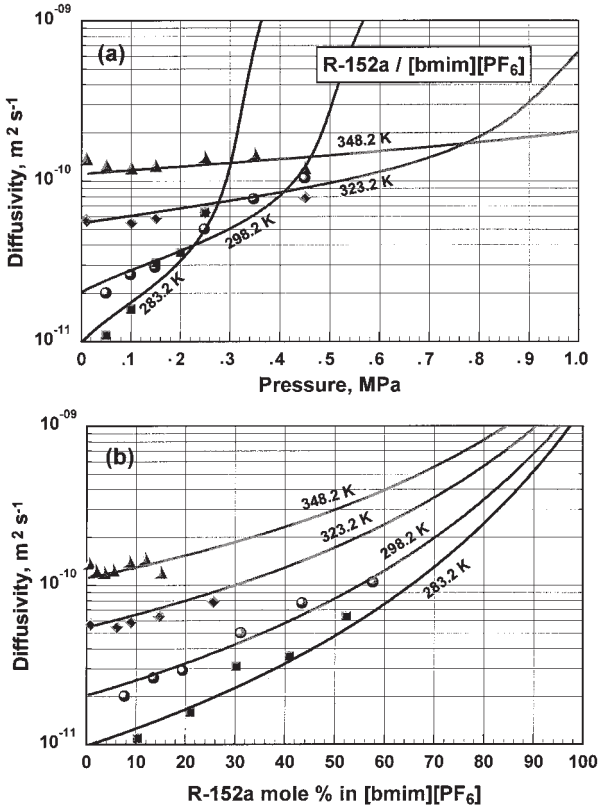

Figure 7. Diffusivity diagrams of R-152a in [bmim][PF_6].

(a) Diffusivity vs. pressure; (b) diffusivity vs. composition. Lines: model calculations (see text); symbols: the present experimental data.

correlation (see Figures 3–6). Figure 7 shows both D vs. P and D vs. x plots using a case of the R-152a/[bmim][PF_6] system, whereas the remaining figures (Figures 8–11) show only D vs. P plots. All D vs. x plots are qualitatively similar; D increases with x monotonically without crossing each other. The model calculation is generally in good agreement with the experimental data (within a factor of ~2), which are often scattered with rather large uncertainties.

It is interesting to see that the b parameters in Table 10 for ionic liquid solutions have magnitudes similar to those established in various nonelectrolyte solutions,[9] between 0.5 and 1.0. The empirical a parameter in Eq. 34 can possess a physical meaning: $a = \ln(k/6\pi r\eta_0)$. If the present model with Eq. 33 or 34 is physically meaningful, the determined a parameters should provide reasonable values in r (effective molecular radius of solute), or at least a physically correct order of magnitude. Values from −27.1 to −28.2 in a (see Table 10) give r = 0.43 to 1.29 nm, which are indeed physically reasonable values, compared with molecular diameters (0.33–0.46 nm) of HFCs (R-23, R-32, R-125, R-134a, R-143a, and R-152a).[18] It is expected that the molecular size of CO_2 will be the smallest among the systems studied here. Indeed, r values in CO_2 are the smallest: r (in [bmim][PF_6]) = 0.229 nm and r (in [bmim][BF_4]) = 0.295 nm. These values are adequately compared with a reported molecular radius of CO_2, which is about 0.20 to 0.23 nm, based on the molecular diameter of CO_2.[19]

Discussion

In this article, we have discovered large differences in the solubility among HFCs in an ionic liquid, [bmim][PF_6]. Similar solubility behaviors will be expected for HFCs in other ionic liquids such as [bmim][BF_4], some of which have been studied in this work. At first glance, these solubility differences are surprising, by considering the fact that the same types of compounds usually show similar VLE (solubility) behaviors in a given type of solvent. HFC compounds are known to possess large electric dipole moments (or highly polar compounds) and ionic liquids, which may also be regarded as highly polar solvents, are likely to explain the observed solubility behavior. However, the magnitude of the electric dipole moment of HFCs does not correlate the observed solubility trend. The dipole moments of R-152a, R-143a, R-134a, R-125, R-32, and R-23 are 2.262, 2.340, 2.058, 1.563, 1.978, and 1.649 debye, respectively,[11,18] whereas R-32 is most soluble and R-143a is least soluble; or the solubility order in solvent-rich side solutions is R-32 > R-152a > R-23 > R-134a > R-125 > R-143a (see Figure 1).

Another unique property in HFCs is their H-bonding capability (H—F—H), although their role in the present solubility behavior is not obvious. It is also interesting to observe that CO_2 is also characterized by fairly high solubility, at least in [bmim][PF_6]-rich side solutions, as shown in Figure 1. CO_2 is nonpolar (no electric dipole moment), although it possesses a relatively large quadrupole moment,[22] and has π electrons

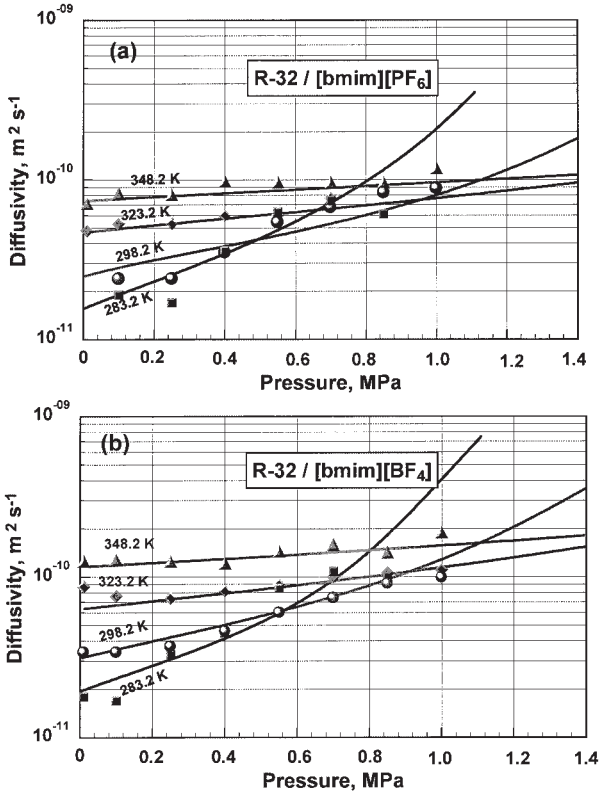

Figure 8. Diffusivity diagrams of R-32.

(a) Diffusivity vs. pressure in [bmim][PF_6], and (b) diffusivity vs. pressure in [bmim][BF_4]. Lines: model calculations (see text); symbols: the present experimental data.

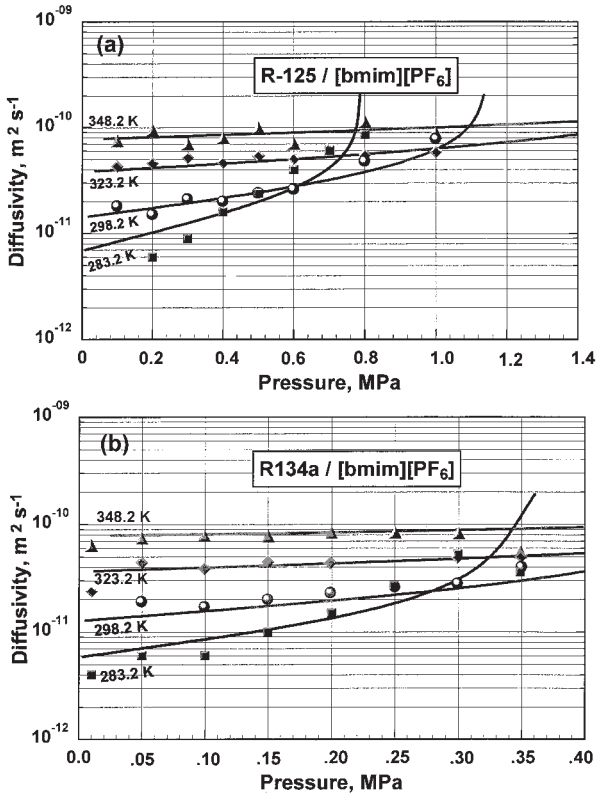

Figure 9. Diffusivity diagrams.

(a) Diffusivity vs. pressure of R-125 in [bmim][PF_6]; (b) diffusivity vs. pressure of R-134a in [bmim][PF_6]. Lines: model calculations (see text); symbols: the present experimental data.

(conjugated double bonds). Charge-transfer complex formations, solvations of ions, and molecular associations, among other phenomena, may be involved, but at present no specific or integrated intermolecular forces are identified as being responsible for the observed solubility behavior.

Although we do not have a clear understanding on a molecular level, the present solubility difference can be used for engineering processes such as extractive distillations or extraction solvents.[16] Both binary mixtures of R-32/R-125 and R-125/R-143a are azeotropic systems and important refrigerants. Purification or reuse of these refrigerants as recovery products will be particularly suited with the present ionic liquids because of the significantly large solubility differences.

All solubility (VLE) data of the present binary systems with ionic liquids have been successfully correlated with the conventional activity models for nonelectrolyte solutions. However, the present results are not surprising, given that several successful attempts using nonelectrolyte models for electrolyte solutions have been published in the literature.[13-16] Treating the ionic liquid as an undissociated species may not be a bad assumption in the present case. Most of the electrolyte-solution models assume the complete dissociation, which is, however, not always a correct assumption. With respect to the phase behavior correlation, it seems well established that nonelectrolyte-solution models work well even for electrolyte solutions.[15]

The prediction of LLE based on only VLE data, or vice versa, is not numerically accurate in the conventional activity models.[8] However, it is interesting to show that the present NRTL model analyses predict LLE for the case of ionic liquid mixtures with R-143a and CO_2 (see Figure 12). The predicted phase behaviors will be correct, at least qualitatively, and it is also predicted that the immiscibility gap (of LLE) decreases as T decreases, indicating that it has a lower critical solution temperature (LCST). A similar phase behavior was predicted in our previous report on CO_2/ionic-liquid systems.[10] However, it should be mentioned here that the present activity models (or any solution models, Eq. 12) is inaccurate (or undefined) at high temperatures, particularly near and above T_c of gaseous species. Thus, extrapolations for phase behaviors over wide temperature ranges must be treated with great caution. More reliable predictions of large-scale (global) phase behaviors may be made using proper equations of state, which are reported in a separate paper,[23] where we show that binary HFC and CO_2 systems with the present ionic liquids belong to the category of Type V fluids, according to the classification of Scott and van Konynenburg.[22,26,27]

Another interesting prediction with the present NRTL solution model is about the thermal property [that is, excess properties of Gibbs (G^E), enthalpy (H^E), and entropy (S^E) functions]. An example is shown in Figure 13, using R-134a/[bmim][PF_6]. The excess H^E and S^E values can be derived from G^E [17]:

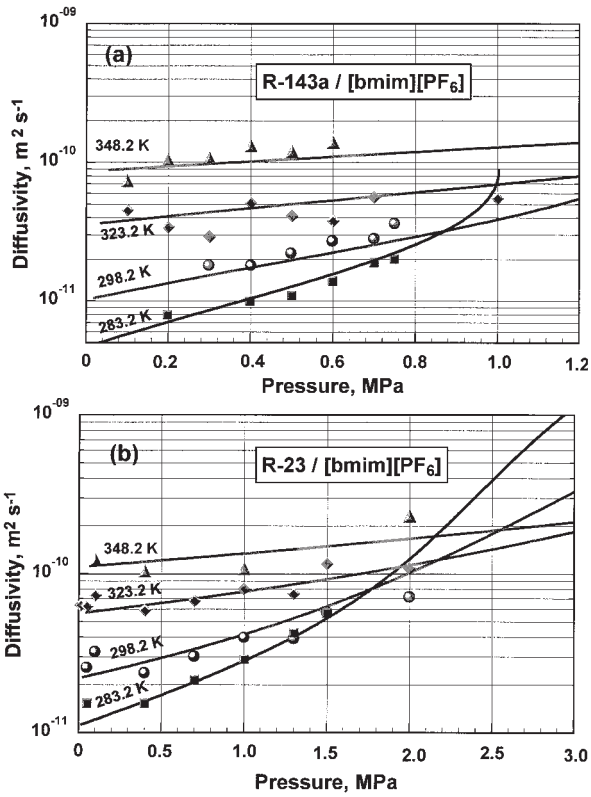

Figure 10. Diffusivity diagrams.

(a) Diffusivity vs. pressure of R-143a in [bmim][PF_6]; (b) diffusivity vs. pressure of R-23 in [bmim][PF_6]. Lines: model calculations (see text); symbols: the present experimental data.

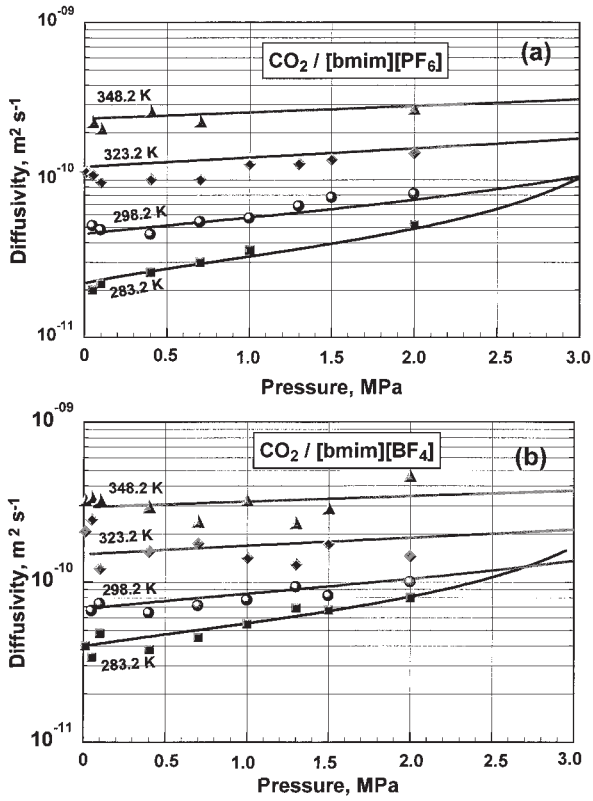

Figure 11. Diffusivity diagrams of CO_2.

(a) Diffusivity vs. pressure in [bmim][PF_6]; (b) diffusivity vs. pressure in [bmim][BF_4]. Lines: model calculations (see text); symbols: experimental data.[10]

$$\frac{G^E}{RT} = \sum_{i=1}^{2} x_i \ln \gamma_i \tag{38}$$

$$\left(\frac{\partial [G^E/RT]}{\partial T}\right)_{P,x} = -\frac{H^E}{RT^2} \tag{39}$$

or

$$H^E = -RT^2 \sum_{i=1}^{2} x_i \left(\frac{\partial \ln \gamma_i}{\partial T}\right)_{P,x} \tag{40}$$

$$TS^E = H^E - G^E \tag{41}$$

The excess G^E function can be quite accurately predicted when the VLE (P, T, x) data are well correlated. In fact, the three activity models (Margules, Wilson, and NRTL) provided a nearly identical G^E function because the P–T–x curves by these models are very close to each other (see Figure 2). However, accurate predictions for both H^E and S^E are very difficult. This is because they are derived from the temperature derivative of the activity coefficient and the T dependency in any activity model is always a purely empirical form. Figure 13 shows only the results by the NRTL model and both H^E and S^E by the Margules and Wilson models for this binary system agree only qualitatively with those by the NRTL results. Therefore, discussions about the excess enthalpy and entropy are necessarily qualitative. It is observed that both H^E and S^E in Figure 13 are negative in the [bmim][PF_6]-rich side solution, whereas in the R-134a–rich side both become largely positive as the system temperature increases, suggesting lower solubility as the temperature increases.

Finally, it is gratifying to see that the observed diffusivity behaviors (in D vs. P, or D vs. x plots) have been well explained by a simple diffusion model, developed in the present study. The model is based on the theoretical Stokes–Einstein model plus a well-known empirical relation between solution viscosity and diffusivity,[9] and the solution viscosity model is taken from our previous work.[20] As discussed in the diffusivity modeling section, the empirical fitting parameter, a in Eq. 34, may contain a physically meaningful quantity: that is, the size of the diffusing body. In fact, in the case of CO_2 in ionic liquids, the present model (a) provided a molecular size that is remarkably close to the known CO_2 molecular size.[19] The question then arises concerning other systems. If we take seriously the present model parameter a numerically, based on the results of CO_2, the size of diffusing bodies of all HFCs in the ionic liquids is a few times larger than the typical molecular size of HFCs.[18] In particular, the smallest molecular size among all HFCs studied here is R-32, but the derived diffusing body size is the largest: fivefold (in [bmim][BF_4]) to eightfold (in [bmim][PF_6]) times larger than the known size of R-32.[18] It is intriguing to imagine that R-32 (or other HFCs) diffuses in

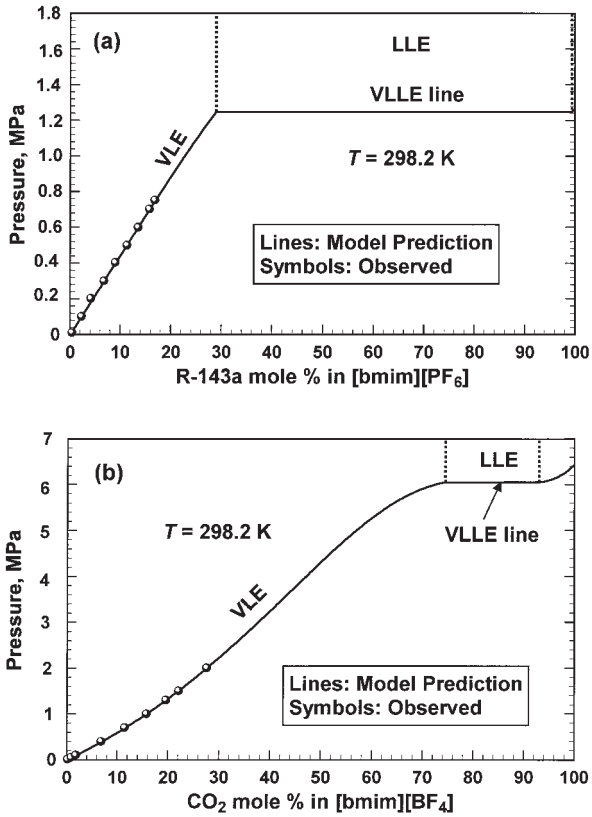

Figure 12. Predictions of phase behaviors by the present NRTL model at 298.2 K.

(a) R-143a/[bmim][PF_6]; (b) CO_2/[bmim][BF_4].

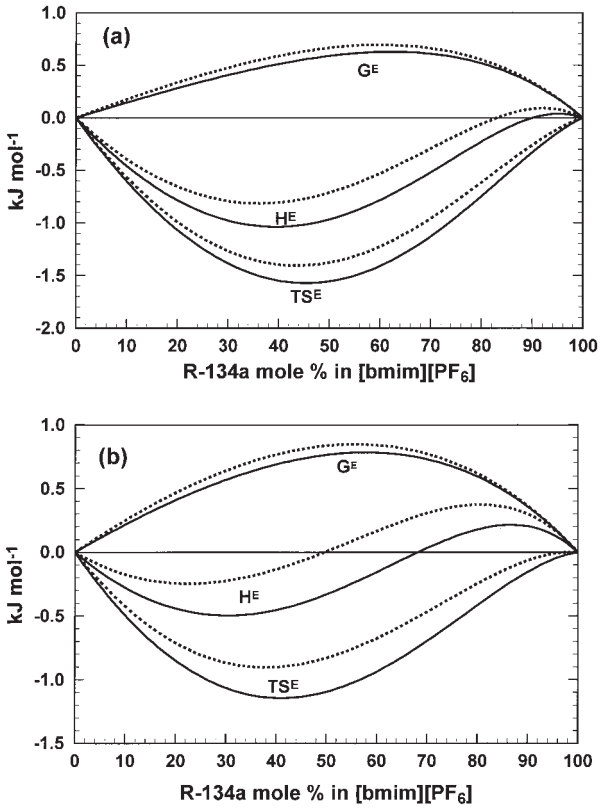

Figure 13. Predictions of the excess Gibbs, enthalpy, and entropy functions for R-134a/[bmim][PF_6] mixtures by the present NRTL model.

(a) T = 283.2 (solid lines) and 298.2 (dotted lines) K; (b) T = 323.2 (solid lines) and 348.2 (dotted lines) K.

ionic liquids as clusters (or molecular associations). Some spectroscopic experiments might prove such behaviors.

Conclusions

We have studied the solubility and diffusivity of an important class of compounds—hydrofluorocarbons (HFCs)—in commonly known ionic liquids: [bmim][PF_6] and [bmim][BF_4]. To our best knowledge, these studies have not previously been reported in the literature. We have found amazingly different solubilities among HFCs in ionic liquids. Although the mechanism of the solubility difference is not clear at an intermolecular level, the engineering applications projected from the present discovery are quite significant in the field of material separations among HFCs, such as extractive distillation and extraction solvents.

The observed VLE (P, T, x) behaviors of electrolyte (ionic liquid) solutions with HFCs have been well correlated with the conventional solution (activity coefficient) models for nonelectrolyte solutions.

Diffusivity data of HFCs in the ionic liquids are obtained for the first time in this work. The observed behaviors of the isothermal diffusivity in the pressure or composition space have been successfully correlated with a model developed in this study.

Acknowledgments

The authors thank Brian L. Wells for conducting the experiments and Seun S. Solesi for assistance in obtaining the diffusivity data at the DuPont Experimental Station. The present work was supported by DuPont Central Research and Development as a discovery-research project (no. 530059).

Notation

a, b = adjustable parameters, generalized Stokes–Einstein equation, Eqs. 33 and 34
A, B = Margules activity model binary interaction parameters, Eqs. 16 and 17
A_I, B_1, C_1 = Antoine constants, where T is in K and P_1^s is in MPa, Eq. 15
A_i, B_i, C_i, D_i = viscosity constants, where T is in K and η_i is in mPa·s or cP, Eq. 37
B_i = second viral coefficient of ith species, m^3 mol^{-1}
c = adjustable parameter, mass vs. mole fraction, Eq. 36
C_0 = initial concentration, mol m^{-3}
C_s = saturation concentration, mol m^{-3}
$\langle C \rangle$ = space-averaged concentration, mol m^{-3}
D = diffusion constant, m^2 s^{-1}
f = fugacity, MPa
G^E = excess Gibbs free energy, kJ mol^{-1}
H = Henry's constant, bar (10 × MPa)
H^E = excess enthalpy, kJ mol^{-1}
k = Boltzmann constant, 1.38048 × 10^{-23} J K^{-1}
L = length, m
m_i, M_i = molecular weight of ith species, kg $kmol^{-1}$
N = total number of components
p_{ij} = binary interaction parameter
P_i = pressure of ith species, MPa
r = radius, m
R = gas constant, 8.31434 J mol^{-1} K^{-1}
S^E = excess entropy, kJ mol^{-1} K^{-1}
t = time, s
T_c = critical temperature, K
$\tilde{V}_i$ = molar volume of ith species, cm^3 mol^{-1} (or m^3 mol^{-1})
$\Delta\tilde{V}$ = change in molar volume, cm^3 mol^{-1} (or m^3 mol^{-1})
w_i = weight of ith species, kg
x, y = mole fraction of ith species

Greek letters

α = constant, Eq. 5
α, τ_{12}, τ_{21}/α, Δg_I, Δg_2 = NRTL activity model binary interaction parameters, Eqs. 25 and 26
ξ_i = variable defined in Eq. 36
Φ_i = correction factor of ith species
γ_i = activity coefficient of ith species
λ_n = eigenvalue, m^{-1}
ρ_i = density of ith species, kg m^{-3}
η = viscosity, cP, 10^{-3} Pa·s
Λ_{12}, $\Lambda_{21}/\lambda_{12}$, $\lambda_{21}/\Delta\lambda_1$, $\Delta\lambda_2$ = Wilson activity model binary interaction parameters, Eqs. 19–22
G_{12}, G_{21}, τ_{12}, τ_{21} = NRTL activity model binary interaction parameters, Eqs. 23 and 24

Subscripts

A = dilute solute A
B = solvent B
g = gas
i = ith species
L = liquid
m = mixture
s = saturation
0 = initial, or ionic liquid
1 = sample gas
2 = ionic liquid

Superscripts

~ = molar property

E = excess property
s = saturated property
(0) = temperature-independent constant, Eqs. 27–30
(1) = temperature-dependent constant (K), Eqs. 27–30
(2) = temperature-dependent constant (K^{-1}), Eq. 27

Literature Cited

1. Walden P. Molecular weights and electrical conductivity of several fused salts. *Bull Acad Imper Sci St Petersburg* 1914;405:22.
2. Wilkes JS, Zaworotko MJ. Air and water stable 1-ethyl-3-methylimidazolium based ionic liquids. *J Chem Soc Chem Commun.* 1992;965.
3. Solvent Innovation. http://www.solvent-innovation.com. Solvent Innovation GmbH, Cologne, Germany; 2005.
4. Holbrey JD, Seddon KR. Ionic liquids. *Clean Products Process.* 1999; 1:223–236.
5. Shariati A, Peters CJ. High-pressure phase behavior of systems with ionic liquids: Measurements and modeling of the binary system fluoroform + 1-ethyl-3-methylimidazolium hexafluorophosphate. *J Supercrit Fluids.* 2003;25:109-117.
6. Abbott AP, Eardley CA, Harper CJ, Hope GE. Electrochemical investigations in liquid and supercritical 1,1,1,2-tetrafluroroethane (HFC 134a) and difluoromethane (HFC 32). *J Electroanal Chem.* 1998;457: 1-4.
7. Abbott AP, Eardley CA. Conductivity of $(C_4H_9)_4N\ BF_4$ in liquid and supercritical hydrofluorocarbons. *J Phys Chem B.* 2000;104:9351-9355.
8. Walas SM. *Phase Equilibria in Chemical Engineering.* Boston, MA: Butterworth; 1985:178-183.
9. Reid RC, Prausnitz JM, Poling BE. *The Properties of Gases and Liquids.* 4th Edition. New York, NY: McGraw-Hill; 1987.
10. Shiflett MB, Yokozeki A. Solubilities and diffusivities of carbon dioxide in ionic liquid: [bmim][PF_6] and [bmim][BF_4]. *Ind Eng Chem Res.* 2005;44:4453-4464.
11. Lemmon EW, McLinden MO, Huber ML. A computer program, REFPROP (Reference Fluid Thermodynamic and Transport Properties, ver. 7). Gaithersburg, MD: National Institute of Standards and Technology; 2002.
12. Yokozeki A. Time-dependent behavior of gas absorption in lubricant oil. *Int J Refrig.* 2002;22:695-704.
13. Kato R, Krummen M, Gmehling J. Measurement and correlation of vapor–liquid equilibria and excess enthalpies of binary systems containing ionic liquids and hydrocarbons. *Fluid Phase Equilib.* 2004; 224:47-54.
14. Döker M, Gmehling J. Measurement and prediction of vapor–liquid equilibria of ternary systems containing ionic liquids. *Fluid Phase Equilib.* 2005;227:255-266.
15. Anderko A, Wang P, Rafal M. Electrolyte solutions: From thermodynamic and transport property models to simulation of industrial processes. *Fluid Phase Equilib.* 2002;194/197:123-142.
16. Seiler M, Jork C, Kavarou A, Arlt W, Hirsch R. Separation of azeotropic mixtures using hyperbranched polymers or ionic liquids. *AIChE J.* 2004;50:2439-2454.
17. Van Ness CH, Abbott MM. *Classical Thermodynamics of Nonelectrolyte Solutions.* New York, NY: McGraw-Hill; 1982.
18. Yokozeki A, Sato H, Watanabe K. Ideal-gas heat capacities and virial coefficients of HFC refrigerants. *Int J Thermophys.* 1998;19:89-127.
19. Hirschfelder JO, Curtiss CF, Bird RB. *Molecular Theory of Gases and Liquids.* New York, NY: Wiley; 1964:1111.
20. Yokozeki A. Solubility and viscosity of refrigerant–oil mixtures. Proc of International Computer Engineering Conference, Purdue University, West Lafayette, IN; 1994;1:335-340.
21. Michels HH, Sienel TH. Proc of International Conference on Ozone Protection Technology, Baltimore, MD; 1997:96-105.
22. Rowlinson JS, Swinton FL. *Liquids and Liquid Mixtures.* 3rd Edition. London, UK: Butterworth; 1982.
23. Yokozeki A, Shiflett MB. Global phase behaviors of hydrofluorocarbons in ionic liquids (in preparation); Proc. of 1st Int. Congress on Ionic Liquids, Salzburg, Austria; June 19–22, 2005:112.
24. Geller V, Paulaitis M, Bivens D, Yokozeki A. Transport properties and heat transfer of alternatives for R502 and R22. Proc of ASHRAE/NIST Refrigerants Conference, American Society of Heating, Refrigerating, and Air-Conditioning Engineers; 1996:73-78.
25. Japanese Association of Refrigeration. *Thermophysical Properties of Environmentally Acceptable Fluorocarbons: HFC-134a and HCFC-123*. Tokyo, Japan: Japanese Association of Refrigeration; 1990:61.
26. Scott RL, van Knoynenburg PH. Static properties of solutions. Van der Waals and related models for hydrocarbon mixtures. *Discuss Faraday Soc.* 1970;49:87-97.
27. van Knoynenburg PH, Scott RL. Critical lines and phase equilibria in binary van der Waals mixtures. *Philos Trans.* 1980;A298:495-540.

Manuscript received Apr. 15, 2005, and revision received Aug. 8, 2005.